

# Magnetic fabrics indicating Late Quaternary seismicity in the Himalayan foothills

R. Jayangondaperumal · Ashok Kumar Dubey ·  
B. Senthil Kumar · S. G. Wesnousky ·  
S. J. Sangode

Received: 30 March 2009 / Accepted: 26 October 2009 / Published online: 3 December 2009  
© Springer-Verlag 2009

**Abstract** The anisotropy of magnetic susceptibility (AMS) study was performed on soft sediment samples from a trenched fault zone across the Himalayan frontal thrust (HFT), western Himalaya. AMS orientation of  $K_{\min}$  axes in the trench sediments is consistent with lateral shortening revealed by geometry of deformed regional structures and recent earthquakes. Well-defined vertical magnetic foliation parallel to the flexure cleavage in which a vertical magnetic lineation is developed, high anisotropy, and triaxial ellipsoids suggest large overprinting of earthquake-related fabrics. The AMS data suggest a gradual variation from layer parallel shortening (LPS) at a distance from the fault trace to a simple shear fabric close to the fault trace. An abrupt change in the shortening direction ( $K_{\min}$ ) from NE–SW to E–W suggests a juxtaposition of pre-existing layer parallel shortening fabric, and bending-related flexure associated with an earthquake. Hence the orientation pattern of magnetic susceptibility axes helps in identifying co-seismic structures in Late Holocene surface sediments.

**Keywords** Anisotropy of magnetic susceptibility (AMS) · Earthquake fabric · Himalaya · Paleoseismicity

## Introduction

Recent studies have indicated great surface rupturing earthquakes (1200–1700 AD) in vicinity of the Himalayan frontal thrust (HFT, separating the Indo-Gangetic Alluvial Plain from the Siwalik Group of rocks) in the western Himalaya (Kumar et al. 2006), and in the Nepal Himalaya (1100 AD) (Lave et al. 2005) (Fig. 1) This study is based on trenching of active fault structures (asymmetric folding and/or thrusting) observed in late Holocene terrace/fan deposits (Fig. 2). However, absence of micro-seismicity and historical record of an earthquake associated with the HFT raises question whether the observed structures were formed seismically by an earthquake(s) or aseismically by slow deformation (aseismic fault creep) (Yeats and Hussain 2006). In order to find a solution, we studied meter scale deformation structures in a trenched fault zone (Kumar et al. 2006) at Rampur Ganda (Figs. 1, 2) across the HFT in the western Himalaya using anisotropy of magnetic susceptibility technique (AMS or magnetic fabrics) (Hrouda 1982; Tarling and Hrouda 1993; Borradaile and Henry 1997). One of the main advantages of the technique is that it is a very sensitive method that can detect fabric anisotropies in weakly deformed rocks and soft sediments (Borradaile and Henry 1997).

AMS study has been used extensively for Quaternary deformation and seismotectonic studies (Sagnotti and Speranza 1993; Housen et al. 1996; Sagnotti et al. 1998; Parés et al. 1999; Lee and Angelier 2000; Borradaile and Hamilton 2004; Levi et al. 2005). These studies demonstrate that AMS is an effective tool to distinguish

---

R. Jayangondaperumal · A. K. Dubey (✉)  
Wadia Institute of Himalayan Geology,  
Dehradun 248001, India  
e-mail: akdubey@wihg.res.in

B. Senthil Kumar  
Indian Institute of Sciences, Bangalore, India

S. G. Wesnousky  
Center for Neotectonic Studies, University of Nevada,  
Reno, NV 89577, USA

S. J. Sangode  
Department of Geology, University of Pune, Pune, India

**Fig. 1** **a** An outline map of the Himalaya showing prominent Himalayan thrusts and locations of recent study areas mentioned in the text (*MCT* main central thrust; *MBT* main boundary thrust; *HFT* Himalayan frontal thrust). The *irregular polygon* shows inferred surface rupture extent of 1200–1700 AD earthquake event (Kumar et al. 2006). **b** A generalized geological N–S cross-section showing major thrusts and main Himalayan thrust across the Nepal Himalaya (after Kumar et al. 2006). Location of the cross-section shown in Fig. 1a by a *solid line* connecting two *black squares* (N–S)

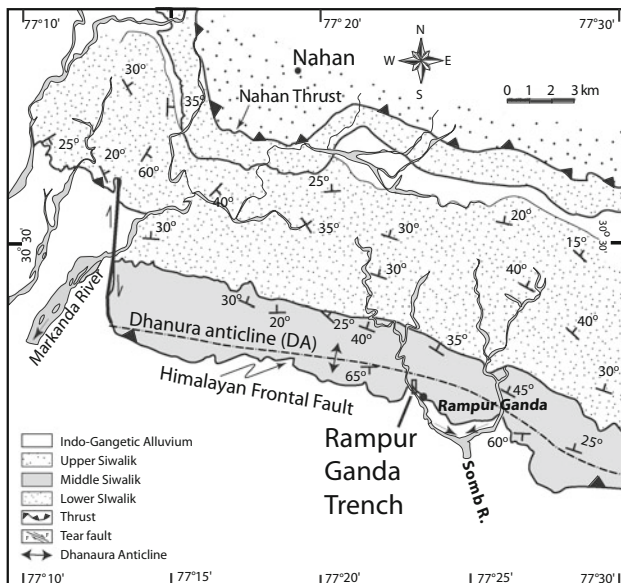
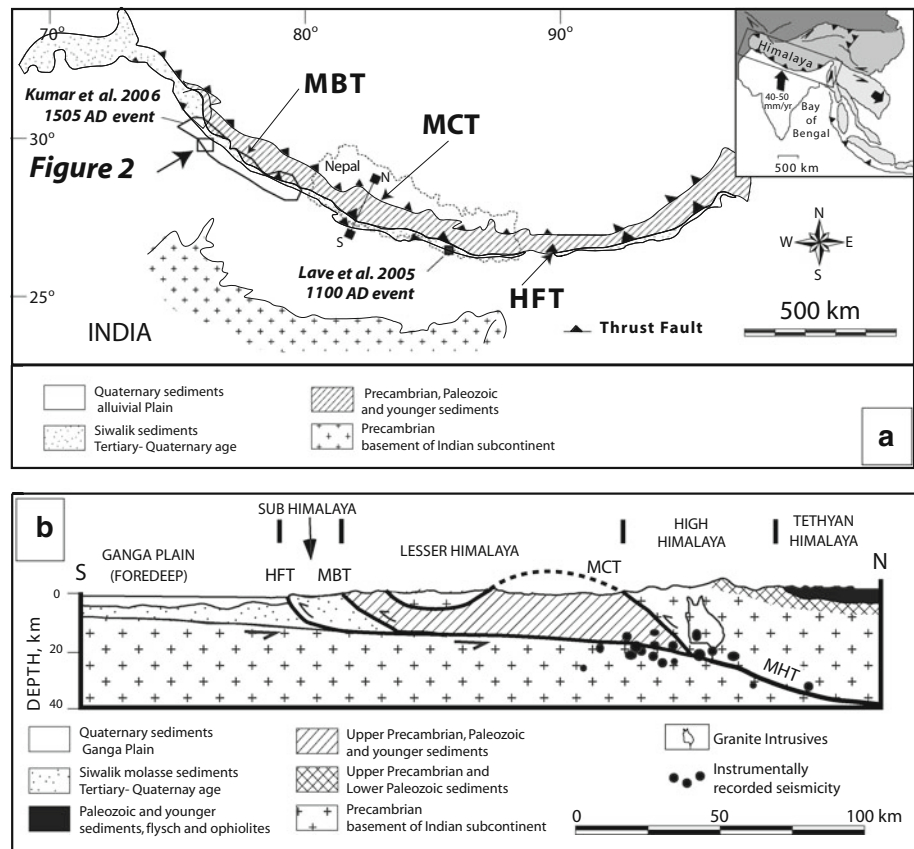


**Fig. 2** A geological map of part of the Himalayan foothill belt showing location of Rampur Ganda trench site (modified after Kumar et al. 2006)

components of sedimentary fabric (resulting from compaction) and earthquake-induced structures. AMS has been used to characterize soft sediment deformation (Schwehr and Tauxe 2003) as it can unravel the finite strain ellipsoid

orientation in weakly deformed sediments and rocks, where tectonic fabric has not developed (Borradaile and Henry 1997; Parés 2004). Levi et al. (2006) have analyzed sedimentary and seismic origin of clastic dikes in the Dead Sea basin and observed that AMS can be used as an effective tool for paleoseismic records.

AMS has also been used as a strain gauge, and several quantitative relationships have been reported from studies on different tectonic environments (Rathore 1980; Kligfield et al. 1981, Hirt et al. 1988; Borradaile 1988; Hroudá 1982; Borradaile and Henry 1997). Despite a large number of useful publications, there appears to be a gap in understanding how AMS fabric develops during coseismic faulting, especially in a trench fault zone, which provides an opportunity to examine the deformation path in fold-and-thrust belts (FTBs).

### Geological setting

The Himalayan fold and thrust belts have formed as a result of collision between the Indian and the Eurasian plates. The region is characterized by three major south verging NW–SE-oriented thrust faults that dip 30–45° toward NE and extend ~2,500 km along the length of the Himalaya (Fig. 1; Gansser 1964). The northernmost, highest, and

oldest main central thrust zone (MCT) marks a tectonic contact between the High Himalayan crystalline and the Lesser Himalayan rocks. South of the MCT, the main boundary thrust (MBT) marks a tectonic contact between predominately pre-Tertiary Lesser Himalayan meta-sediments, and Tertiary and Quaternary sub-Himalayan sediments (Valdiya 1992). The southernmost thrust that lies in the study area is known as the HFT, which separates the Tertiary and Quaternary sediments from modern alluvium of Indo-Gangetic Plain along its entire length (Nakata 1972). Expression of the HFT in the young alluvium is in the form of short, discrete, and discontinuous range front scarps that displaces the Quaternary alluvial fans and terraces (Nakata 1972; Valdiya 1992; Wesnousky et al. 1999; Kumar et al. 2006). All these thrust faults merge into a common decollement zone known as the Main Himalayan thrust (MHT) (Fig. 1b; Seeber and Armbruster 1981; Nelson 1998). The study area lies in foothills of the sub-Himalaya which consists of Lower, Middle and Upper Siwaliks folded to form the NW–SE striking Dhanura anticline (DA). Both DA and HFT are locally curved especially at the exit of the Somb River (Fig. 2).

#### Rampur Ganda trench site

Rampur Ganda trench site (Fig. 2) is located in the southern forelimb of the NW trending DA. The foreland (south) verging anticline consists of gray to brown sandstone and mudstone of Middle Siwalik Formation dipping 30–40° NE and overlie the Indo-Gangetic Alluvial Plain along the HFT. The discontinuous trace of the scarp is 8 m high and strikes WNW–ESE to NW–SE. Figure 3 shows a log of the eastern trench wall. The log shows two depositional units (2a and 2b) that lie unconformably over a mudstone (unit 1). Unit 2a is composed of rounded to sub-rounded cobble and boulder gravel. The uppermost unit 2b is clayey silt of flood plain deposits. The unit is thick in the northeast, taper to cm thickness near the inflection of the scarp, and disappears because of erosion of the scarp. A sub-vertical extensional fault (F4–F4') with funnel shape geometry at the top striking NNW–SSE was observed in units 2a, 2b and 1. Unit 2b appears to have collapsed over the fault (Fig. 3). In unit 1, closely spaced steep fracture or flexure cleavage striking NNW–SSW with sub-vertical dip toward NE was observed. These structures presumably accommodate a part of the bending (Kumar et al. 2006). The dipping units (dip 16° toward south) form a ramp parallel to the morphology of the scarp. The sequence is cut by a set of three thrusts—F1, F2, and F3 (striking NW–SE, dip varying from 23 to 33° toward NE). In the footwall of the scarp unit 2b' consists of consolidated massive dark clayey silt. Units 3 and 3' are continuous units of the scarp derived colluvium that caps unit 2b'. The minimum observed displacement along different

stands F1, F2, and F3 is about 7 m with vertical separation of about 8 m (Fig. 3c). A detailed paleoseismic investigation and its seismotectonic implication was described by Kumar et al. (2006).

## Methods and samples

### Anisotropy of magnetic susceptibility (AMS)

AMS measures the bulk-preferred orientation of ferromagnetic, paramagnetic, and diamagnetic minerals and/or crystal lattices (Hrouda 1982). It is expressed as second order symmetric tensor with three principal susceptibility axes referred as  $K_{\max} > K_{\text{int}} > K_{\min}$ . Orientations of the susceptibility axes are closely related to petrofabric strain axes ( $X > Y > Z$ ) and can be proportional to the magnitude of finite strain (Borradaile 1991) in strong to weakly deformed rocks, where penetrative fabrics have not developed. The relationship between finite strain and magnetic fabric is complex, but this can be understood by studying deformation environment and origin of AMS using appropriate instruments (Borradaile and Henry 1997). The transition from compaction fabrics to strain fabrics shows large changes (Housen et al. 1993; Parés et al. 1999) that have to be critically evaluated for reliable application of magnetic analyses to deformed rocks. Nevertheless, the consensus has been that magnetic lineation is parallel to extension direction (magnetic lineation =  $K_{\max}$ ), and orientation of  $K_{\min}$  axis is parallel to shortening direction (Borradaile and Henry 1997; Housen et al. 1996; Aubourg et al. 1999; Sagnotti et al. 1994; Parés et al. 1999).

The various scalar anisotropy parameters used in the present study are; lineation factor ( $L = K_{\max}/K_{\text{int}}$ ), foliation factor ( $F = K_{\text{int}}/K_{\min}$ ), degree of anisotropy ( $P_j$ ), and shape parameter ( $T$ ). The  $P_j$  is intrinsic anisotropy that either reflects the degree of alignment of minerals as a function of strain intensity or magnetic mineralogy, which is linear to bulk susceptibility ( $K_m$ ) (Borradaile 1988; Parés and van der Pluijm 2002). The shape factor or shape parameter ( $T$ ) is described as:  $T > 0$ , oblate;  $T = 0$ , triaxial; and  $T < 0$ , prolate (Jelinek 1981; Tarling and Hrouda 1993).

Oriented block samples were extracted from the eastern trench wall (Fig. 3) following the procedure described by Tarling and Hrouda (1993). Thirteen sites (169 cubes with 2 cm sides) were sampled from the Siwalik mud stone (unit 1), and consolidated clayey silt (unit 2b'). These units are suitable for study of AMS because they are compact and relatively hard. Each sample yielded 16–22 specimens (Table 1). The samples (13 sites) were collected systematically from NE to SW with respect to observed structural

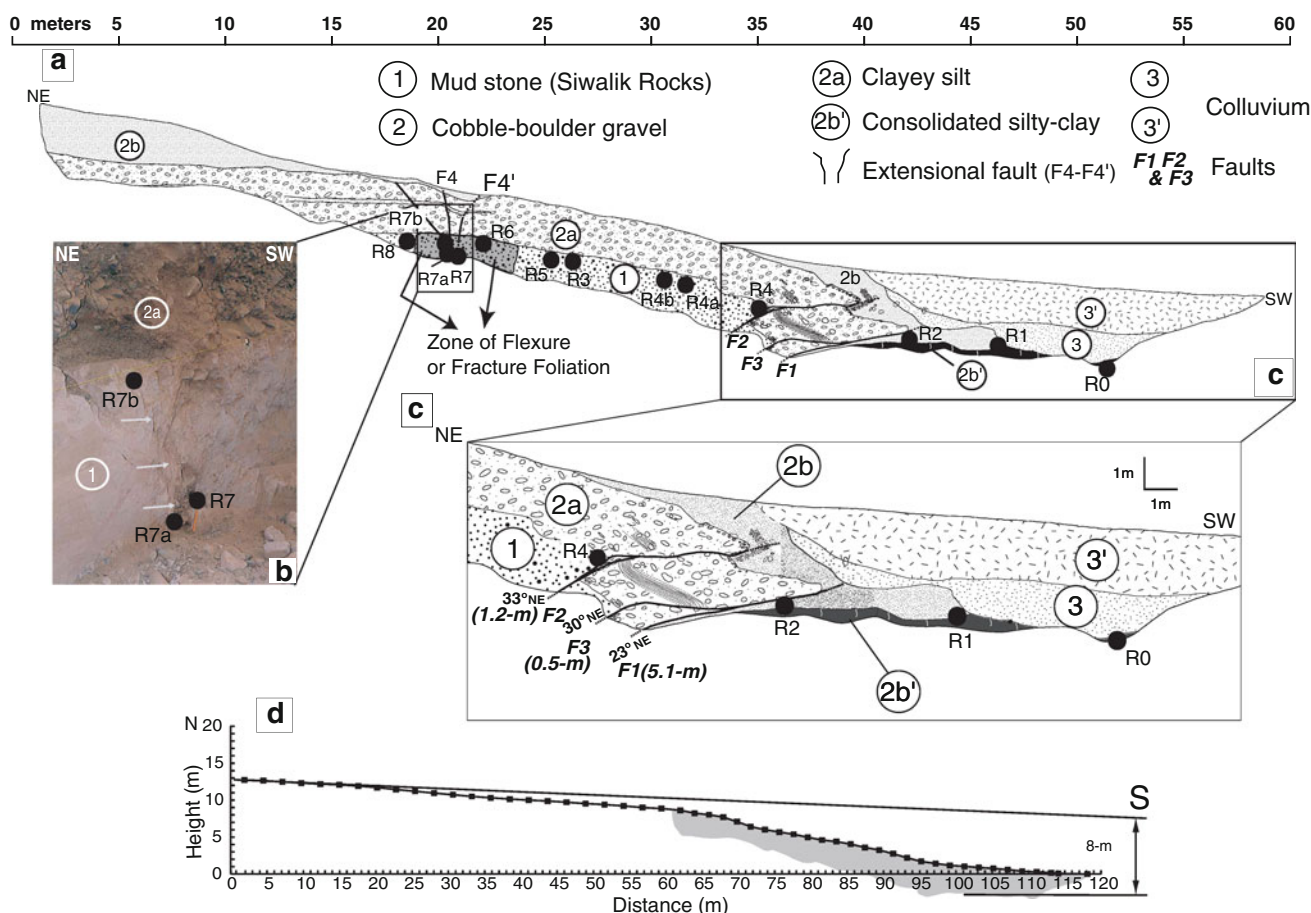


**Fig. 3** a Eastern wall of Rampur Ganda trench site showing deformed structures and AMS sample sites. Gray area within unit-1 shows zone of fracture cleavage. b A vertical extensional fault (F4–F4′) located at the trailing end of the thrusts with AMS sample sites.

White arrows represent flexure foliation. c Enlarged view of the trench log showing directions of faults, and AMS sites. d The scarp profile within the trench area is marked in gray

discontinuities and their locations as follows (Fig. 3). Sites R0, R1, and R2 were collected from the consolidated clayey silt unit (2b′) at the footwall. Of these sites, R2 was collected immediately beneath the F1 fault, and R0 at SW termination of the trench. R1 was collected 1 m from the fault tip (F1) located between the sites R0 and R2. R4 was collected on the F2 fault trace from the hangingwall unit of chocolate to brown mud stone (unit 1). R4a and R4b, collected from the same unit, are located less than 5 m from the site R4, toward NE. R3 and R4 were collected between the 25- and 30-m marks toward NE of unit 1, away from faults F1–F3 and extensional faults F4–F4′. Site R6 is located close to the F4–F4′ fault zone, whereas sites R7, R7a, and R7b are located within the faults zone. Inside the fault zone, NNW–SSE striking fracture foliation or flexure foliation oblique to the bedding plane is predominant. Site R8 is located between the 15- and 20-m marks, 2 m from the F4–F4′ fault zone, toward NE.

AMS was measured with a KLY 3S Kappabridge (at Paleomagnetic Laboratory, Wadia Institute of Himalayan

Geology, Dehradun) and various parameters ( $P_j$ ,  $T$ ,  $L$ ,  $F$ ,  $K_m$ ,  $K_{mean}$ , declination and inclination component of principal susceptibility axes  $K_{max}$ ,  $K_{int}$ , and  $K_{min}$ ) were obtained by software supplied with the instrument (Jelinek 1977; Hrouda et al. 1990).

An essential analysis for AMS is to determine the magnetic carriers for magnetic susceptibility and in weakly magnetic rocks whether the AMS tensor is of phyllosilicate or ferrimagnetic nature. Therefore, we applied the routine rock magnetic analysis (isothermal remanent magnetization and anhysteretic remanence) to 20 representative specimens of each site at room temperature using Bartington’s MS-2B system, ASC Scientific impulse magnetizer, Molspin spinner and AFD (alternating field demagnetizer) with ARM (anhysteretic remanent magnetization) facility.

The samples were analyzed by remanence hysteresis and anhysteresis methods, thermal demagnetization of remanence, and anisotropy of ARM. The remanence hysteresis, commonly known as isothermal remanence magnetization

**Table 1** Tensorial mean of AMS parameters for trenched fault zones

Site	<i>N</i>	<i>K<sub>m</sub></i>	<i>L</i>	<i>F</i>	<i>T</i>	<i>P<sub>j</sub></i>	<i>K<sub>max</sub></i> <i>D/I</i>	<i>K<sub>int</sub></i> <i>D/I</i>	<i>K<sub>min</sub></i> <i>D/I</i>
R0	22	248E–06	1.008	1.012	0.0926	1.021	186/15	5.2/13.6	96.5/19
		99E–06	0.011	0.016	0.456	0.025			
R1	21	353E–06	1.050	1.047	0.0251	1.102	330/81	1.0/1	100/13
		373E–06	0.043	0.032	0.242	0.071			
R2	18	404E–06	1.032	1.035	0.065	1.069	336/82	180/4	90/1
		110E–06	0.018	0.017	0.159	0.035			
R3	11	138E–06	1.078	1.096	0.061	1.185	353/86	182/3	91/6
		46E–06	0.039	0.055	0.195	0.099			
R4	3	183E–06	1.090	1.119	0.120	1.222	341/84	174/7	82/4
		69E–06	0.027	0.046	0.033	0.083			
R4'	3	262E–06	1.014	1.067	0.287	1.0926	4/2	125/75	267/13
		67E–06	0.009	0.046	0.020	0.043			
R4a	8	196E–06	1.015	1.016	–0.225	1.032	356/12	89/15	227/70
		24E–06	0.005	0.008	0.385	0.006			
R4b	8	124E–06	1.021	1.017	–0.162	1.040	19/27	271/16	161/55
		15E–06	0.006	0.010	0.395	0.008			
R5	16	72.8E–06	1.008	1.005	–0.282	1.014	66/54	337/2	246/32
		20E–06	0.003	0.252	0.319	0.005			
R6	13	125E–06	1.129	1.106	–0.069	1.253	341/86	179/3	89/1
		37E–06	0.059	0.038	0.314	0.061			
R7	13	113E–06	1.082	1.104	0.094	1.196	346/83	178/7	88/2
		19E–06	0.017	0.040	0.127	0.057			
R7a	9	127E–06	1.113	1.124	0.074	1.255	343/85	178/5	88/1
		41E–06	0.069	0.047	0.317	0.088			
R7b	13	144E–06	1.099	1.116	0.070	1.229	339/87	176/3	86/1
		40E–06	0.038	0.046	0.237	0.067			
R8	12	62.6E–06	1.008	1.011	0.233	1.020	31/76	146/6	235/12
		54E–06	0.005	0.004	0.357	0.006			

Lower rows correspond to standard deviation

*N* number of core samples; *K<sub>m</sub>* volume susceptibility in SI unit; *L* (lineation factor) =  $K_{\max}/K_{\text{int}}$ ; *F* (foliation factor) =  $K_{\text{int}}/K_{\text{min}}$ ; *T* shape factor; *P<sub>j</sub>* corrected degree of anisotropy parameters; *K<sub>max</sub>* *D/I*, *K<sub>int</sub>* *D/I*, *K<sub>min</sub>* *D/I* declination and inclination of magnetic susceptibility axes

(IRM), was analyzed by inducing an incremental magnetic field of 1,500 mT in forward direction and –100 mT in backward direction. This enabled identification of magnetic minerals that are responsible for AMS and their influence on AMS fabrics. In addition, R0 and R1 from the footwall unit 2b', and R5, R6 and R7 from the hangingwall unit 1 were analyzed by X-ray diffraction for identification of phyllosilicates.

## Results

### Magnetic mineralogy

The lower values of volume ( $K_{\text{m}} < 400 \times 10^{-6}$  SI units) and mass specific susceptibility ( $\chi_{\text{lf}} < 3.3 \times 10^{-8}$  m<sup>3</sup>/kg)

for all the studied samples suggest low ferrimagnetic content hence predominance of paramagnetic susceptibilities for which the anisotropy can be controlled by phyllosilicate minerals (Tarling and Hrouda 1993) (Fig. 4). On the other hand, the low susceptibilities may also arise from presence of antiferromagnetic oxides such as hematite and goethite. The slope and under saturation of the partial IRM's till 2,500 mT confirms the presence of antiferromagnetic minerals in majority of the samples (Fig. 4b). The antiferromagnetic mineral hematite shows a strong anisotropy to its basal plane, but it is often randomly oriented in fluvial environments while the goethites do not show any significant anisotropy (Dunlop and Özdemir 2001). The plot  $B_{\text{OCR}}$  versus  $\chi_{\text{lf}}$  (Fig. 4) indicates two major magnetic mineral assemblages grouped as I and II. Group I corresponds to Siwalik mudstone rock of unit 1 and group

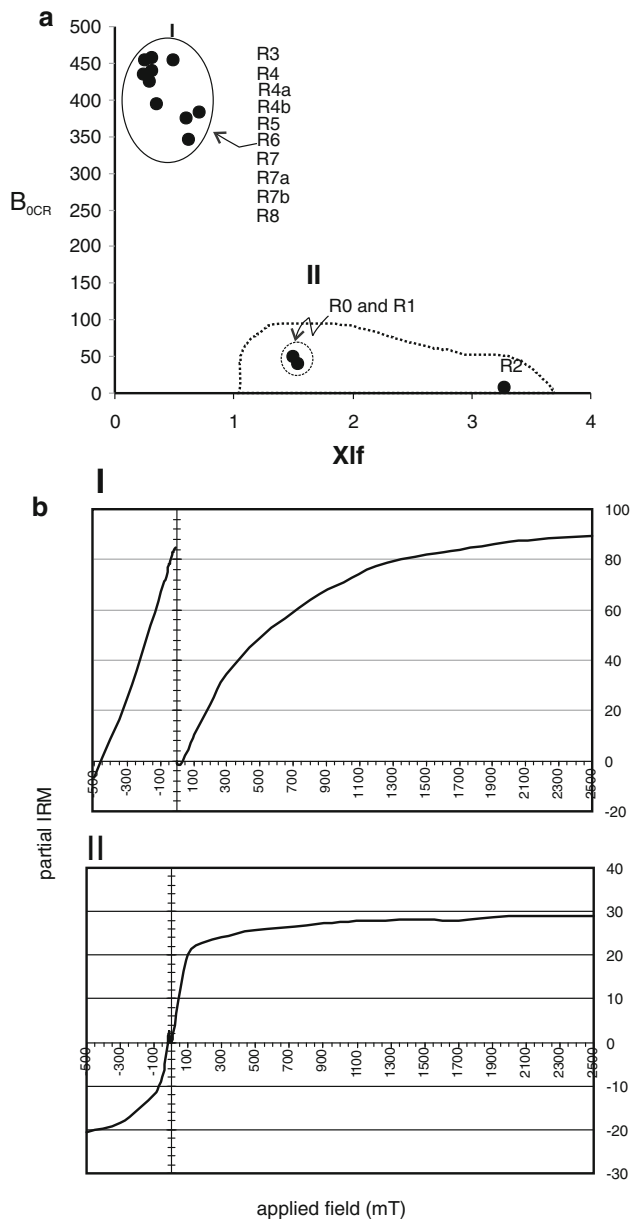


**Fig. 4** **a** Mass specific susceptibility ( $\chi_{Irf}$ ) versus coercivity ( $B_{0CR}$ ) plot for representative specimens from each site. Distinct clusters are based on mineral magnetic variations and are described in the text. **b** The remanence hysteresis loop presented for one specimen of each group showing saturation and coercivity characteristics. The X-axis represents the applied field (mT) in forward and reverse direction, and the Y-axis represents the partial IRM's in  $10^{-5} \text{ AM}^2/\text{kg}$

II corresponds to consolidated massive dark clayey silt of unit 2b' (Fig. 3). Majority of the samples in group I shows very high coercivity ( $>375 \text{ mT}$ ) indicating the presence of hematite and goethite. Samples R0 and R1 in group II show  $B_{0CR}$  and ARM values characteristic of SD (single domain) ferrimagnetic composition. The SIRM values are  $<10 \times 10^{-5} \text{ A m}^2/\text{kg}$  for majority of the samples except for R2 which shows soft coercivity and the

highest susceptibility indicating presence of MD (multi domain) ferrimagnetic grains at relatively higher concentration. The rock magnetic study suggests that none of the magnetic carriers (ferri- or anti-ferromagnetic) plays an important role in producing the anisotropy. Rather the weak susceptibilities but significant anisotropies point toward the phyllosilicate control mainly from those derived from metamorphic source of the Himalayan hinterland.

The degree of anisotropy ( $P_j$ ) obtained by AMS is a control of both the minerals present (defined as mineral anisotropies) and their degree of alignment (Parés and van der Pluijm 2002). In addition Rochette et al. (1992) have inferred that at the susceptibility range of  $K_m$  (mean)  $> 500 \times 10^{-6} \text{ SI}$  unit ferrimagnetic minerals completely dominate the susceptibility. The bulk susceptibility ( $K_m$ ) of all the samples is  $<400 \times 10^{-6} \text{ SI}$ , and does not correlate linearly and positively with the degree of anisotropy  $P_j$  (Fig. 5), suggesting feeble magnetic interaction, if any, among ferrimagnetic grains. There is no linear correlation between changes in bulk susceptibility and the anisotropy parameters ( $P_j$ ,  $L$ , and  $F$ ) indicating absence of magnetic interaction between the ferromagnetic grains (cf. Borradaile 1988). X-ray diffraction attest the abundance of phyllosilicates (especially biotite,  $A^\circ = 2.12$  and  $4.42$ ) in group I of the Siwalik rocks (unit 1), and magnetite in group II. Thus, AMS fabric of the Siwalik mudstone (unit 1) is essentially dominated by phyllosilicates with small amounts of low susceptibility/high coercivity antiferromagnetic minerals, while unit 2b' is dominated by both SD and MD ferrimagnets.

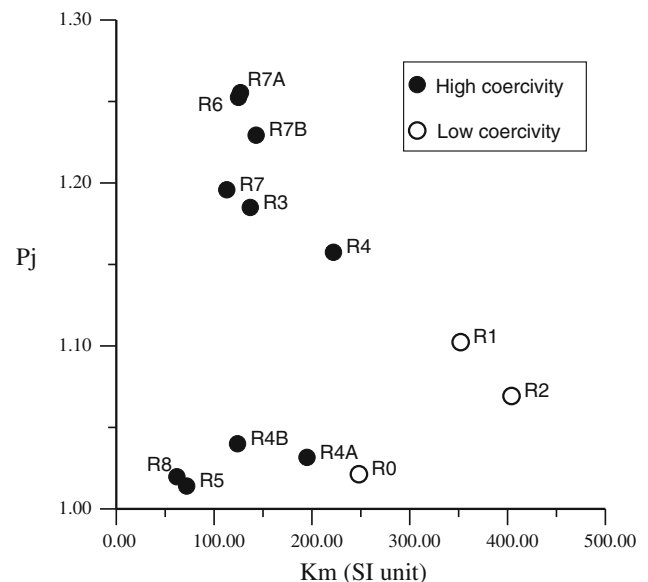


**Fig. 5** Variation of the bulk mean susceptibility in  $K_m$  ( $10^{-6} \text{ SI}$  unit) with degree of anisotropy ( $P_j$ )

## Magnetic fabrics

Figure 6a shows eastern wall of the trench log along with 13 sites of magnetic fabric data. Magnetic fabrics observed along the profile from SW to NE (undeformed footwall to deformed hangingwall) (Figs. 6, 7) are described here. The magnetic fabric at site R0 shows a large scatter, but site R2 shows moderate clustering with scattered susceptibility axes. The scattering is due to presence of both single and multi domain magnetite as indicated by rock magnetic and XRD analyses. Therefore, these sites are excluded from detailed interpretation of AMS parameters and their orientations. Site R4 shows two sub-fabrics: (1) gentle or horizontal plunging magnetic lineation ( $K_{\max}$ ) (R4' in Table 1; Figs. 6b, 7, 8, and (2) steep magnetic lineation (R4 in Table 1; Figs. 7, 8). A careful examination of these two sub-fabrics (Figs. 6b, 7) reveals that the anisotropy value of gently plunging magnetic lineation shows lower  $P_j$  (1.0926) and shape parameter ( $T = 0.287$ ) indicative of oblate ellipsoid (R4' in Fig. 7; Table 1). The steep magnetic lineation shows higher anisotropy ( $P_j = 1.222$ ) and shape parameter ( $T = 0.120$ ) toward triaxial ellipsoid (R4' in Fig. 7; Table 1). AMS ellipsoids of the sites R3 to R6 show strong variation from oblate-triaxial ellipsoids to moderately prolate shapes ( $T = 0.0613$  to  $-0.022$ ; Fig. 7). The degree of anisotropy ( $P_j$ ) varies from 1.014 to 1.040 with exception of higher anisotropy at sites R3 and R6. In contrast, sites R7–R7b show abrupt increase in  $P_j$  ranging from 1.196 to 1.255 and shape parameter ( $T = 0.233$ – $0.070$ ) close to triaxial ellipsoid. At site R8, the AMS ellipsoid shows moderate oblate shape ( $T = 0.233$ ) with low anisotropy ( $P_j = 1.020$ ).

Similar variations were noticed in orientations of magnetic susceptibility axes along the NE–SW profile (Fig. 6). Site R4 shows gentle and steep plunges of  $K_{\max}$  axes (Fig. 6b). At this location a well-developed slaty cleavage parallel to the bedding ( $S_0 = S_1$ ) with two sets of magnetic foliation can be deduced by joining the planes containing the gentle and steep plunges of  $K_{\max}$ – $K_{\text{int}}$ . The gentle  $K_{\max}$  lies within the bedding plane, while the steep  $K_{\max}$  is normal to the bedding fabric. One of the specimens shows steep  $K_{\min}$  which is normal to the slaty cleavage, and two specimens show steep  $K_{\text{int}}$  axes. However, the remaining gentle  $K_{\min}$  axes lie within the slaty cleavage oriented in E–W direction. At R4a site, the magnetic foliation is oblique or sub-parallel to the bedding fabric or slaty cleavage. The gentle  $K_{\max}$  is oriented in N–S direction, and the  $K_{\min}$  is sub-vertical, normal to the slaty cleavage. A small girdle pattern forms between the  $K_{\min}$  and  $K_{\text{int}}$  axes. At R4b site, the magnetic foliation is oblique to the bedding or slaty cleavage, and  $K_{\max}$  is aligned parallel to the intersection lineation along NE–SW direction, whereas  $K_{\text{int}}$  and  $K_{\min}$  forms a girdle pattern. Similar

fabrics are also seen at site R5. At R3 site,  $K_{\max}$  is vertical in the vertical magnetic foliation, and no slaty cleavage was observed. The zone of intermixing between the fracture cleavage and the slaty cleavage was observed between R3 and R6 sites. Site R5 shows both fracture and slaty cleavages, whereas R3 site shows only fracture cleavage. In contrast, R6–R7 displays the same orientations of magnetic susceptibility axes away and within the fracture or flexure foliation zones of F4–F4' fault. Here, the bedding and flexure or fracture foliations are oblique, oriented along NNW–SSE with sub-vertical dip toward NE. A steep  $K_{\max}$  lies within the vertical N–S oriented magnetic foliation. The axis is sub-parallel to fracture foliation, and oblique to bedding fabrics. The gently plunging  $K_{\min}$  axis is oriented along E–W direction. At R8 site, a faint fracture foliation is sub-parallel to the NW striking vertical magnetic foliation. The bedding is oblique to fracture foliation dipping toward NE. The plunge of  $K_{\max}$  is sub-vertical, while the gentle plunge of  $K_{\min}$  axis is along NE–SW direction. At sites R4a, R5, and R8, the orientation of  $K_{\min}$  axes are parallel to the NE–SW regional shortening direction in agreement with the north–east dipping thrusts. At these sites  $K_{\max}$  axes are also clustered along NE–SW to N–S direction, and the observed magnetic lineation is interpreted as being parallel to regional thrust transport direction (i.e. NE–SW). This is in good agreement with the NE trending fault lineation (trend  $30^\circ$ , plunge  $45^\circ$  SW) at site R5. Near the fault strand F2, the  $K_{\min}$  is oriented NE–SW with sub-vertical to vertical dips (R4a). The plunge of  $K_{\min}$  is gentle (R5) or horizontal (R8) oriented along NE–SW direction at a distance from the fault strands, and is interpreted as parallel to the regional shortening direction (NE–SW). Figure 8 shows two groups of ellipsoids: the first group is moderately oblate to neutral, while the second group ranges from very low prolate to triaxial ellipsoids. In general, the plot shows triaxial ellipsoids, especially at sites, located near the fault trace. R4 site located on the F2 fault trace shows two trends (R4 and R4') (Fig. 8): (1) the more oblate shape ( $T = 0.287$ ) with less  $P_j$  (R4'), and (2) more triaxial shape ( $T = 0.12$ ) with higher anisotropy ( $P_j = 1.222$ , R4).

## Discussion and interpretation

A review of existing literature on AMS in the fold-thrust belts suggests four fabric types (Aubourg et al. 1991, 1999; Housen et al. 1996; Borradaile and Henry 1997; Parés et al. 1999; Parés 2004; Robion et al. 2007) based on orientations of  $K_{\max}$  and  $K_{\min}$  axes with respect to observed structural features. The first type is sedimentary fabric, which is characterized by clustering of  $K_{\max}$  within the bedding plane at right angle to the shortening direction. In this case,  $K_{\min}$  is parallel to the bedding pole or girdle distribution

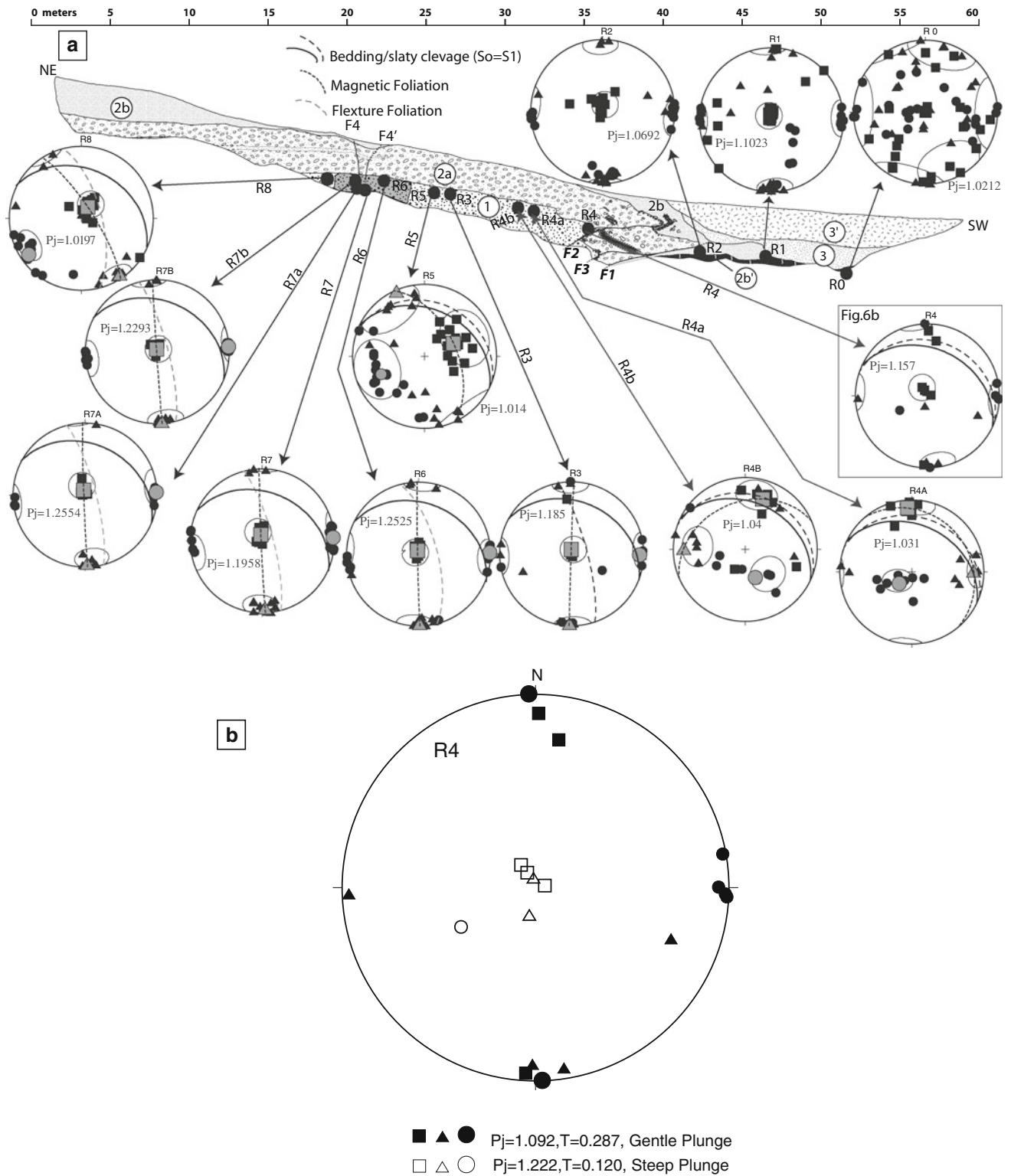


**Fig. 6 a** Eastern wall of the trench showing locations of samples, orientations of magnetic susceptibility axes (equal area lower hemisphere projection), and respective  $P_j$  (corrected degree of anisotropy) values. *Black square*  $K_{max}$ ; *gray square* mean  $K_{max}$ ; *black triangle*  $K_{int}$ ; *gray triangle* mean  $K_{int}$ ; *black circle*  $K_{min}$ ; *gray circle* mean  $K_{min}$ . Sites R6–R7b show magnetic foliation parallel to flexure or fracture foliation. **b** Lower hemisphere equal area plot

showing susceptibility axes of site R4 located on the F2 fault strand showing two sub-sets of AMS fabrics: (1) Magnetic susceptibility axes with lower  $P_j$  are represented by *solid squares, triangles, and circles*. Greater oblate shapes correspond to gentle plunge. (2) Magnetic susceptibility axes with higher  $P_j$  are represented by *hollow squares, triangles, and circles*. Triaxial shape corresponds to steep plunge



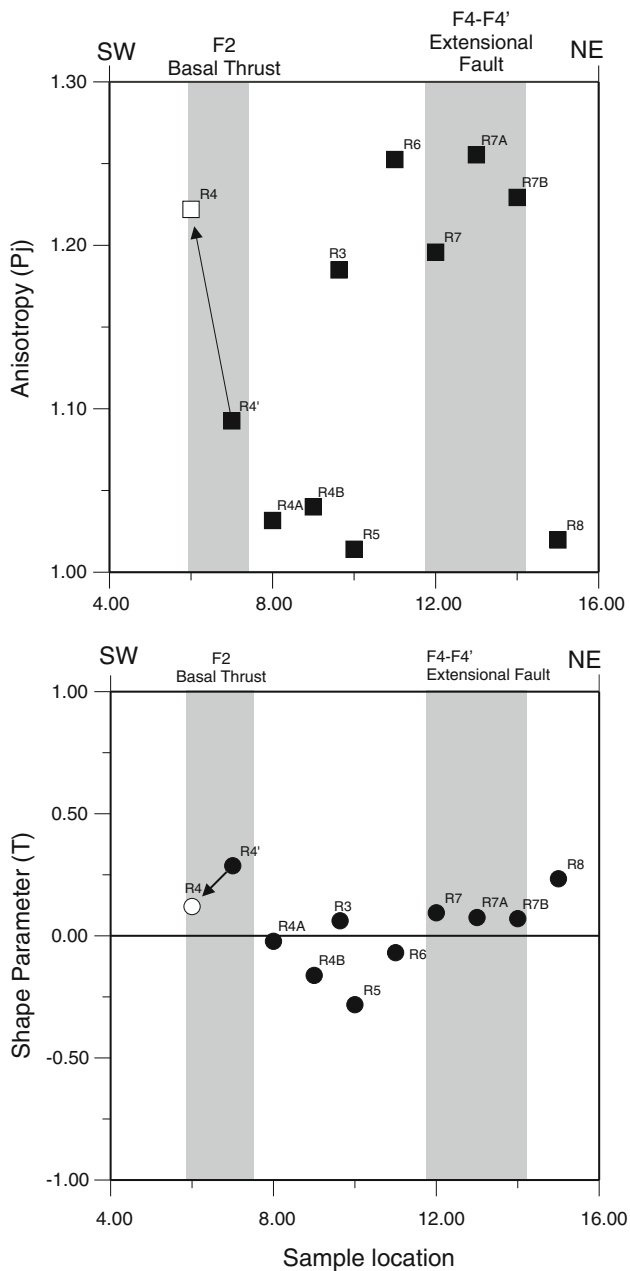


**Fig. 7** Variations of anisotropy degree ( $P_j$ ) (top) and shape parameter ( $T$ ) (bottom) for site locations (4–16) across the trench from SW to NE. Gray area corresponds to fault zones observed in the trench. R4–R4' refers to sub-fabric parameters of R4 site

about  $K_{\max}$ . The second type is referred as intermediate fabrics in which  $K_{\max}$  axis is parallel to the fold axis (Kissel et al. 1986), and  $K_{\min}$  is either parallel to the bedding pole or girdle distribution about  $K_{\max}$ . The third type is characterized by clustering of  $K_{\min}$  axis along the maximum compression direction (Borradaile 1991). In weakly deformed rocks, this type is often associated with development of cleavage or cleavage fabrics (Parés 2004). The last type is characterized by clustering of  $K_{\max}$  along thrust

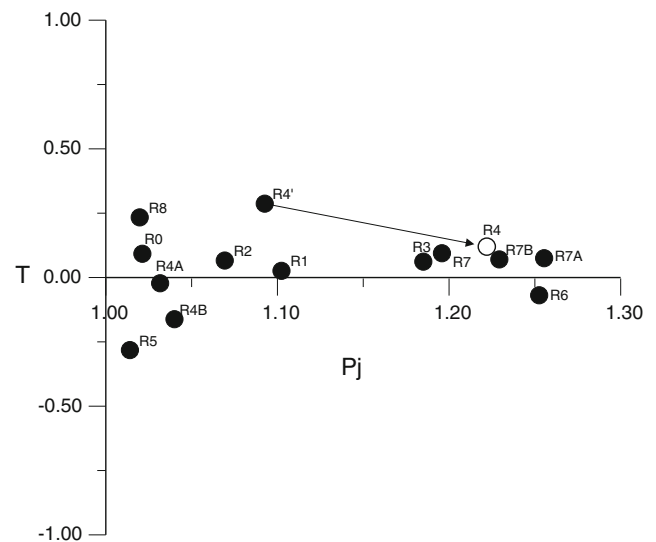


**Fig. 8** Jelinek shape plot showing eccentricity of magnetic ellipsoids with degree of anisotropy ( $P_j$ ). Sites located close to structural discontinuities exhibit triaxial ellipsoid field. R4–R4' refers to sub-fabric parameters of the R4 site

transport direction.  $K_{\max}$  is related to down dip magnetic lineation with clustering or little scatter of  $K_{\min}$  axes that aligns parallel to the shortening direction. This type is often associated with bedding parallel simple shear (R5, R4a, and R4b; Fig. 6) as reported from other fold-thrust belts (Aubourg et al. 1991, 1999). This fabric type is equivalent to Groups V and VI described by Robion et al. (2007) but with a difference that clustering of  $K_{\max}$  axis is within the bedding plane and tendency toward triaxial ellipsoid (cf. Fig. 8). It is to be noted that various AMS studies in the FTBs have shown that these fabric types were evolved from sedimentary to intermediate fabrics reaching eventually to the tectonic fabric (Parés et al. 1999; Parés 2004; de Wall and Warr 2004; Robion et al. 2007). However, in the present example, variation of fabrics was observed within fault zones as summarized below.

The overall AMS fabrics lead to visualization of two end members: (1) a sudden change in orientation of  $K_{\max}$  from NE–SW to N–S with variation in plunge from gentle to vertical, and (2) change in orientation of  $K_{\min}$  from NE–SW to E–W with variation in plunge from sub-vertical to horizontal (Fig. 6). The  $K_{\min}$  axis is the most sensitive proxy for the maximum shortening direction and it is normal to the field and magnetic foliations (Housen et al. 1996; Lee and Angelier 2000; Schwehr and Tauxe 2003). In phyllosilicate bearing rocks the  $K_{\max}$  is also very sensitive as it shows orientation parallel to the fold axis (Borradaile 1991; Aubourg et al. 1991; Owens 1993; Borradaile and Henry 1997). Hence, we used both  $K_{\min}$  and  $K_{\max}$  axes, and changes in degree of anisotropy ( $P_j$ ) together with shape parameter ( $T$ ) (de Wall and Warr 2004) for

data interpretation and explanation for the abnormal fabric changes within the trench (Figs. 6, 7).

The magnetic fabrics show a well-clustered distribution of axes overprinted by thrust-related shear fabrics with higher anisotropy suggesting that the observed fabric is in response to deformation. The shortening direction (NE–SW) inferred from the  $K_{\min}$  axes of AMS fabric is consistent with recent stress direction obtained from the earthquake (Jayangondaperumal and Thakur 2008) and geodetic data (Banerjee and Burgmann 2002). The degree of alignment of minerals ( $P_j$ ), foliation ( $F$ ) and lineation ( $L$ ) parameters are positively linear with the observed faulting and extensional structures in the trench, suggesting that the tectonic fabric has been overprinted on sedimentary fabric (Figs. 6, 7; Table 1). Thus, observed faults and meter scale folds in the trench are indicative of tectonic imprint over sedimentary fabric.

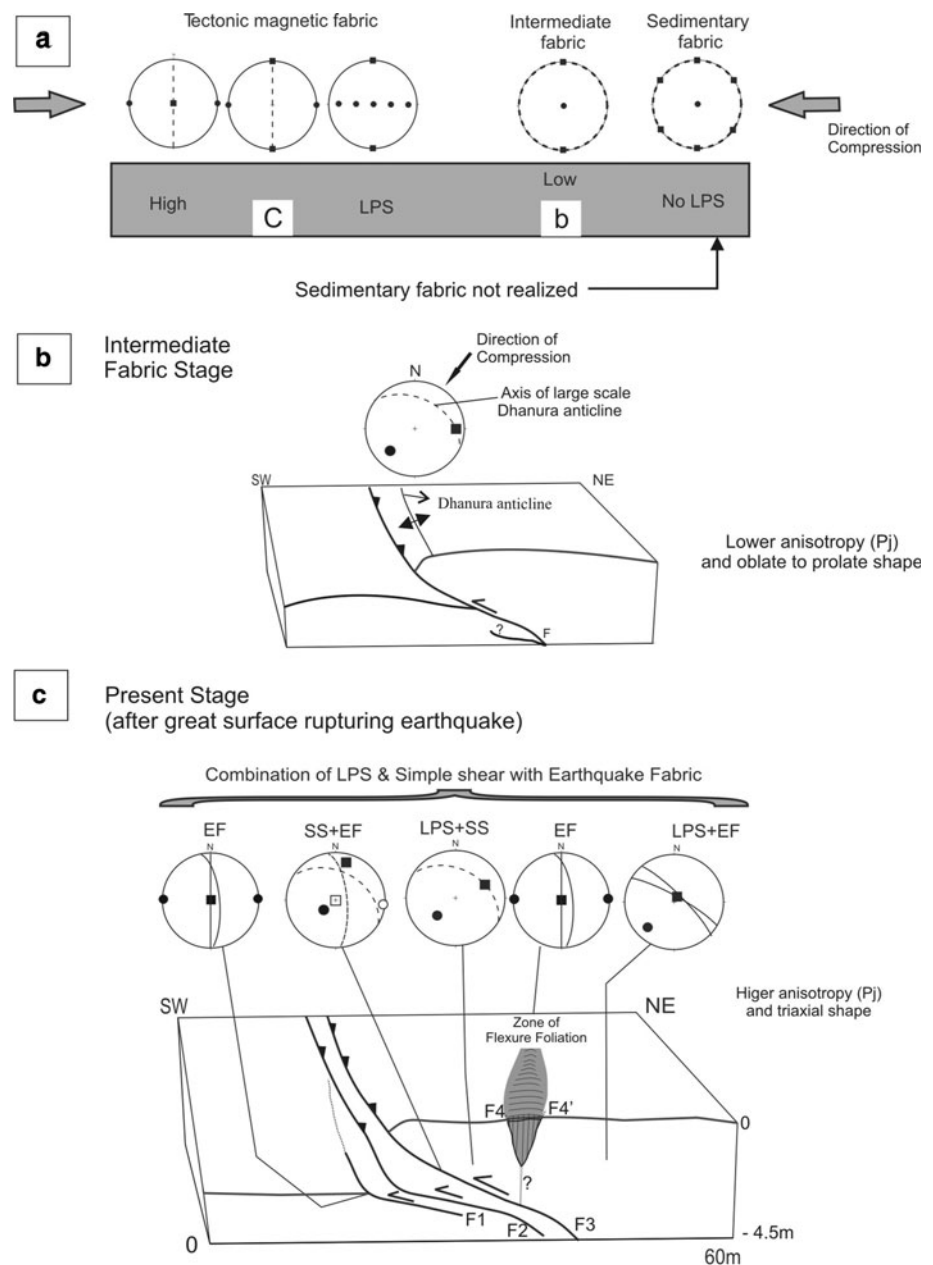
At majority of the sites,  $K_{\min}$  coincides with pole to the bedding and also oblique to the bedding (Fig. 6). This pattern, suggestive of combination of sedimentary and tectonic fabrics, is referred to as composite fabric or Type II (Parés and van der Pluijm 2003). It is to be noted that all previous studies showed grouping of  $K_{\max}$  perpendicular to tectonic shortening direction and  $K_{\min}$  perpendicular or parallel to the bedding. However, in the present example,  $K_{\max}$  is parallel to the thrust transport direction (i.e. NE–SW). The  $K_{\min}$  axes, little scattered and oblique to the bedding, are mostly sub-horizontal and oriented NE–SW, in accordance with the regional shortening direction. In this situation,  $K_{\max}$  becomes thrust transport lineation due to simple shear (e.g. R5, R4a, and R4b) (Aubourg et al. 1991; 1999), and  $K_{\min}$  is parallel to the shortening direction (e.g. R4a, R4b, R5, and R8). Based on the faulting and situation of all sites within the trenched fault zone, the scenario is interpreted as due to simple shear along the basal thrust. This is further evidenced in the Jelinek plot that showed triaxial ellipsoid, especially close to the fault, indicating bedding parallel simple shear (cf. Fig. 8).

To understand the relation between AMS and intensity of grain preferred orientation, Tarling and Hrouda (1993) have estimated the degree of anisotropy ( $P_j$ ) with grain alignment. Subsequently Parés and van der Pluijm (2002) made a single mineral model using  $P_j$  versus degree of mineral alignment. They suggested that this plot provides a relative deformation intensity, as the degree of alignment in a given rock cannot exceed their magnetic values, and thus grains are perfectly aligned due to increase in strain. Similar relation has been observed in samples located on the F2 fault (R4), close to the fault F4–F4' (R6), and within the F4–F4' fault zone (R7–R7b), where anisotropy ( $P_j$ ) is large and their ellipsoids tend to be more triaxial because of shearing along the fault (Fig. 7). Thus, thrusting enhances the anisotropy, and shape parameter becomes

more triaxial ellipsoid. This is very well reflected at site R4 located on the F2 fault trace. As described earlier in the “Results” AMS fabric of the site R4 shows two sub-fabrics, where anisotropy ( $P_j$ ) is low (1.092), and shape parameter ( $T$ ) is slightly oblate for the gentle magnetic lineation. This situation appears to be prior to the earthquake faulting (i.e. low  $P_j$  and more  $T$ ), because sites located away from faults (F1–F4') show gently plunging lineation with low  $P_j$  values (e.g. R4a, R4b, R5 and R8) and sub-horizontal magnetic foliation, lineation, and slaty cleavage. We interpret this stage as intermediate fabric related to growth of the DA, where  $K_{\max}$  is normal to the shortening direction (Fig. 9a, b). Magnetic anisotropies in pelitic rocks are generally low ( $P_j = 1.1$ ) at this stage (cf. de Wall and Warr 2004), and even less than 1.1 has also been reported (Sagnotti et al. 1998). Subsequent to thrusting caused by an earthquake, the magnetic lineation acquires steeper dips, anisotropy increases to 1.222, and ellipsoids acquire triaxial shape (Fig. 9c). Hence both these situations are preserved at site R4 located on the F2 fault trace (Fig. 6). Thus, site R4 showed two sets of magnetic fabrics (gentle and steep plunges of magnetic axes) related to the following.

In general  $K_{\min}$  is oriented normal to the slaty cleavage and thus normal to the magnetic foliation. This implies that prior to faulting or during growth of the DA, the  $K_{\min}$  (one specimen, Site R4; Fig. 6) was normal to the slaty cleavage, and  $K_{\max}$  is gentle and lies within the bedding fabric that was oriented normal to the regional NE–SW shortening direction (Fig. 9b). Consequent to the earthquake faulting,  $K_{\min}$  rotated close to the slaty cleavage along E–W, while  $K_{\max}$  became vertical and normal to bedding and slaty cleavage (Fig. 9c). This interpretation is further tested by examining other sites that are located away from the thrust, where  $K_{\min}$  is normal to the observed slaty cleavage, and  $K_{\max}$  (magnetic lineation) lies either in the bedding or parallel/sub-parallel to the intersection of bedding and magnetic foliation (e.g. R4a, R4b, and R5). Higher anisotropies ( $P_j = 1.15$  and 1.25) are more typical for slaty cleavage with strong preferred orientation of phyllosilicates (e.g. schists in SE Sardinia, Lüneburg et al. 1999; Culm basin in SW England, de Wall and Warr 2004).  $K_{\min}$  and  $K_{\max}$  are very sensitive for small tectonic perturbations (Borradaile and Henry 1997 and references therein), but in the present study we observe changes in the  $K_{\text{int}}$  as well. Thus, anisotropy ( $P_j$ ) has been increased by overprinting of faulting as evidenced at site R4 by F1–F3 faults and at sites R6 through R7b by F4–F4' faults. Sites R3 through R5 located away from the faults F1–F3, and site R8 located away from the F4–F4' faults have showed lower anisotropies (Fig. 7, top panel). As described in the earlier section, the  $P_j$  is controlled by alignment of minerals either by tectonic or by magneto-mineralogy (Parés and van der

**Fig. 9** **a** A schematic representation of evolution of magnetic fabrics and orientation of susceptibility axes with respect to degree of layer parallel shortening (adopted from Saint-Bezard et al. 2002) (equal area lower hemisphere projection). **b** A simplified cartoon depicting intermediate fabric stage during the development of DA. Note that  $K_{\max}$  is aligned normal to the direction of compression. **c** A simplified cartoon of the trench showing earthquake induced fabric pattern. At the back end of the basal thrust within the extensional fault zones F4–F4', a large earthquake fabric shows vertical fracture foliation, magnetic foliation, and magnetic lineation ( $K_{\max}$ ) with EW alignment of the  $K_{\min}$  dominates. *Broken lines* magnetic and slaty cleavage; *solid line* magnetic foliation and flexure or fracture cleavage. Near the basal thrust (F2), AMS fabric shows simple shear (*solid symbols*) and earthquake fabric (EF, *hollow symbols*), whereas away from the basal thrust, simple shear fabric (SS) is overprinted on pre-existing layer parallel shortening (LPS) fabric. The  $K_{\min}$  axis is parallel to the regional shortening direction (NE–SW)



Pluijm 2002; Parés 2004). The rock magnetic studies also suggest that sites R4 and R6–R7b (Unit I, Siwalik rocks) are essentially controlled by paramagnetic minerals, and these sites are within the deformed zone. Hence, the enhancement of anisotropy can be ascribed to intense deformation (Borradaile 1988; Parés and van der Pluijm 2002). Furthermore shape parameter ( $T$ ) for sites R3, R4a, R4b, R5, and R6 located away from the basal faults (F1–F3) showed essentially prolate ellipsoids except at site R6, which is close to triaxial ellipsoid. Similarly site R8 located away from the F4–F4' faults shows more oblate ellipsoids. Site R4 located at fault F2 and within the fault zone F4–F4' (R7, R7a, and R7b) showed a large number of triaxial

ellipsoids (Fig. 7, lower panel). These observations suggest that overprinting by thrusting enhanced the anisotropy and resulted in triaxial ellipsoids otherwise the fabric shows oblate and prolate ellipsoids (e.g. R4b, R5, R6, and R8).

The vertical magnetic lineation ( $K_{\max}$ ) and N–S-oriented vertical magnetic foliations are parallel to the bending related extensional fracture cleavage (sites R6, R7, R7a, and R7b) exposed away from the basal thrust (Fig. 6). However, these sites showed E–W orientation of the  $K_{\min}$  axes that needs to be explained. This can be attributed to three mechanisms: (1) change in shortening direction away from the fault due to superposed deformation (Dubey 2004), (2) the superimposition of layer parallel shortening

(LPS) (Averbuch et al. 1992), and (3) bending-related flexure due to coseismic faulting during a large earthquake (cf. Philip and Meghraoui 1983; Hardebeck and Hauksson 2001; Martinez-Diaz 2002). The possibility of change in shortening direction due to superposed deformation can be ruled out as the observed faults are dipping toward NE; the fold shows NW–SE regional and E–W local trends, and the stress directions derived from a recent earthquake do not support this interpretation (Jayangondaperumal and Thakur 2008).

The LPS related magnetic foliation may have initiated when the bedding was horizontal (cf. Graham 1966; Lee et al. 1990; Averbuch et al. 1992; Sagnotti and Speranza 1993; Parés et al. 1999). In order to confirm this, the bedding was restored to horizontal. The tilt correction for all these sites yielded gentle dipping to horizontal magnetic foliation and  $K_{\min}$  (i.e. shortening direction) roughly parallel to N–S (Fig. 10). This implies that the steep  $K_{\max}$  and E–W orientation of the  $K_{\min}$  axis confined within the fault zones (F1–F4') (Fig. 9c) were formed at a later stage during the earthquake faulting. Sites (R4a, R4b, R5, and R8) situated away from the fault zones (F1–F4) show evidence of layer parallel shortening (LPS) that is responsible for grouping of  $K_{\max}$  accompanied by girdle containing  $K_{\min}$  and  $K_{\text{int}}$  (Sagnotti et al. 1994). Hence, vertical magnetic foliation and magnetic lineation due to superimposition of layer parallel shortening can also be ruled out.

A vertical extensional fault with funnel shape geometry was observed in units 2a and 2b, whereas closely spaced steep fracture cleavages were observed in unit 1. This extensional fault is located at a bend. This suggests that a large opening in the form of funnel geometry changes from extension near the surface (i.e. units 2a and 2b) to compression at depth without offset in unit 1 (i.e. Siwalik). It is to be noted that within the F4–F4' fault zone, NNW–SSE striking closely spaced fracture foliation which is oblique or at high angle to the bedding fabric suggests a compressional structure that needs E–W compression. This is very-well evidenced in the AMS fabric in the form of alignment of  $K_{\min}$  along E–W direction (Fig. 9c). The change in shortening direction from NE–SW to E–W may be related to superposed deformation which is simultaneous with thrusting caused due to change in fault geometry, complex fault interaction (Martinez-Diaz 2002), or occurrence of a large earthquake (Hardebeck and Hauksson 2001) to accommodate a part of bending. Similar interpretation was ascribed to change in the shortening direction in southern California based on inversion of earthquake focal mechanism (Hardebeck and Hauksson 2001). Therefore, considering the regional tectonic setting and geometry of structures, we suggest that surface flexure induced local extension by bending of strata, and sudden

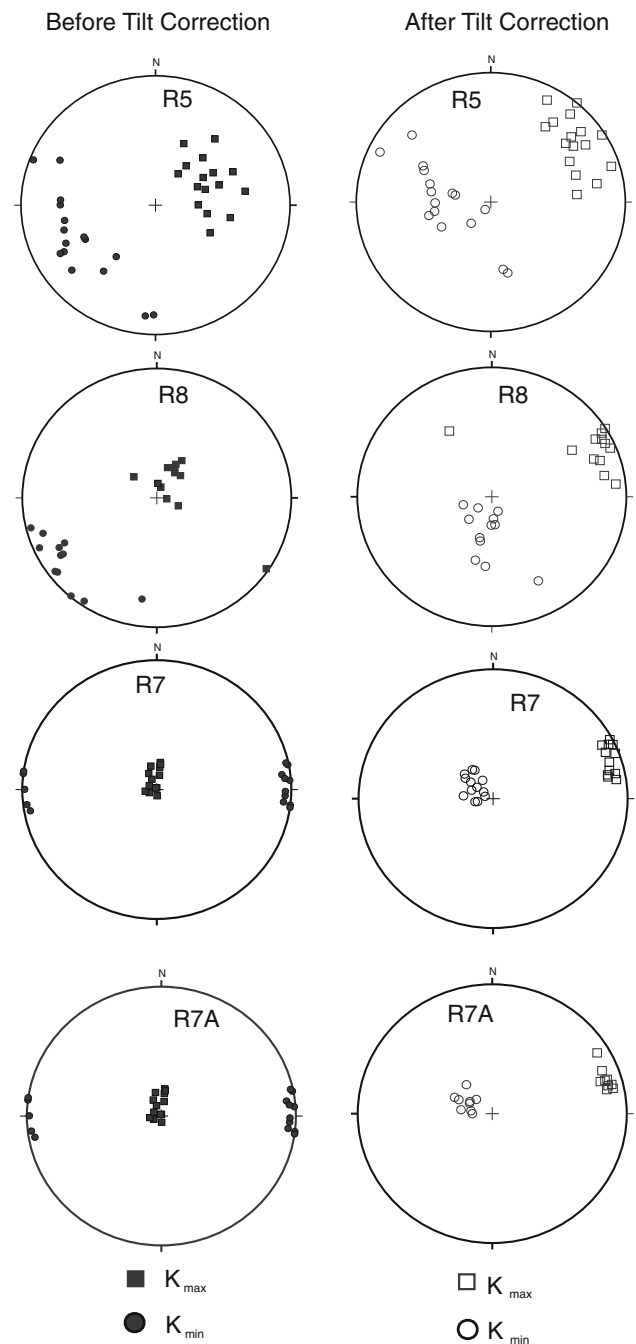


**Fig. 10** Principal susceptibility axes before (*left*) and after (*right*) tilt correction (bedding attitudes restored to horizontal) for selected sites

fall of the overthrusting block was due to a large coseismic faulting as reported earlier in the El Asnam earthquake, West Mediterranean area (Philip and Meghraoui 1983). The E–W horizontal orientation of  $K_{\min}$  axis is perpendicular to NNW–SSE-oriented magnetic foliation observed within the extensional fault. This is related to the flexure formed due to coseismic fault, since it is parallel to the observed structural trend. The bending-related flexure fabric has been juxtaposed with preexisting fabric during

the large earthquake (coseismic faulting) that reorganized the magnetic fabric including: (1) reorientation of  $K_{\min}$  axes into E–W direction, (2) gentle to steep magnetic lineation oriented normal to the  $K_{\min}$ , and (3) gentle NW–SE strike of the magnetic foliation into  $\sim$ N–S vertical foliation (Fig. 9c). The preexisting layer parallel fabric was reoriented by a sudden co-seismic faulting and resulted in vertical magnetic lineation and foliation. This is also suggested for the orientation after the bedding tilt correction, where the magnetic susceptibility axes are horizontal (Fig. 10). Despite the difference in magneto-mineralogy, the magnetic fabric orientation at sites R2 and R1 are the same as in the northernmost samples with steep N–S trending foliation and steep lineation that are interpreted as deformed earthquake fabrics rather than influence of magnetic mineralogy. Similar abrupt change in  $K_{\min}$  axis and increase in  $K_{\min}$  plunge have been reported from the decollement and underthrusting zone in the Barbados accretionary prism (Housen et al. 1996).

If these structures were formed by a slow deformation or by aseismic fault creep, the progressive changes in deformation would have produced the coaxial fabric that could have been reflected in the AMS. However, in the present case it shows non-coaxial and coaxial fabrics together with flexure-related fabrics.

## Conclusions

1. Results of the AMS study are in support of the earlier inference (Kumar et al. 2006) that faulting of the Holocene sediments across the HFT was due to an earthquake with higher magnitude than the historically recorded earthquakes.
2. An abrupt change in declination and inclination of  $K_{\min}$  susceptibility axes, large variation in plunge amount, coaxial fabric at a distance from a fault trace, non-coaxial fabric with vertical magnetic lineation ( $K_{\max}$ ), and vertical magnetic foliation closer to the fault trace suggest coseismic deformation as documented in the present study.
3. A sudden change in orientation of minimum magnetic susceptibility axes ( $K_{\min}$ ) in vicinity of a basal thrust indicates true thrust transport direction, whereas at a distance from the basal thrust the fabric is dominated by pre-to post-thrusting processes.
4. AMS can be an effective tool to detect and measure low strains around faults for paleoseismic records.

**Acknowledgments** We thank Dr. Carlo Dietl, Dr. Helga de Wall, Prof. Wolf-Christian Dullo, and an anonymous reviewer for review comments that helped in revising the manuscript. The trench work was funded by NSF grant No. EAR 9972955 to S. G. Wesnousky. The

authors wish to acknowledge Drs. B. R. Arora, P. Banerjee, V. Sriram and late Professor K. N. Khattri for helpful discussions. Rakesh Kumar assisted in the rock magnetic analysis and Samay Singh in X-ray diffractometry.

## References

- Aubourg C, Rochette P, Vialon P (1991) Subtle stretching lineation revealed by magnetic fabric of Callovian-Oxfordian black shales (French Alps). *Tectonophysics* 185:211–223
- Aubourg C, Rochette P, Stephan JF, Popoff M, Chabert-Pelline C (1999) The magnetic fabric of weakly deformed Late Jurassic shales from the southern sub alpine chains (French Alps): evidence of SW-directed transport direction. *Tectonophysics* 307:15–32
- Averbuch O, Frizon de Lamotte D, Kissel C (1992) Magnetic fabric as a structural indicator of the deformation path within a fold-thrust structure: a test case from the Corbieres (NE Pyrenees, France). *J Struct Geol* 14:461–474
- Banerjee P, Burgmann R (2002) Convergence across northwest Himalaya from GPS measurements. *Geophys Res Lett* 29:13. doi:10.1029/2002GL015184
- Borradaile GJ (1988) Magnetic susceptibility, petrofabrics and strain—a review. *Tectonophysics* 156:1–20
- Borradaile GJ (1991) Correlation of strain with anisotropy of magnetic susceptibility (AMS). *Pageoph* 135:15–29
- Borradaile GJ, Hamilton T (2004) Magnetic fabrics may proxy as neotectonic stress trajectories, Polis rift, Cyprus. *Tectonics* 23 TC1001. doi:10.1029/2002TC001434
- Borradaile GJ, Henry B (1997) Tectonic applications of magnetic susceptibility and its anisotropy. *Earth Sci Rev* 42:49–93
- De Wall H, Warr LN (2004) Oblique magnetic fabric in siderite-bearing polytomic rocks of the Upper Carboniferous Culm Basin, SW England: an indicator for palaeo-fluid migration? In: Martin-Hernandez F, Lüneburg CM, Aubourg C, Jackson M (eds) *Magnetic fabrics: methods and applications*, vol 238. Geological Society of London, Special Publication, pp 493–507
- Dubey AK (2004) Structural evolution of the Himalaya: field studies, experimental models, and implications for seismicity. *Himalayan Geol* 25:33–50
- Dunlop DJ, Özdemir O (2001) *Rock magnetism*. Cambridge University Press, Cambridge
- Gansser A (1964) *Geology of the Himalayas*. Wiley Interscience, London
- Graham JW (1966) Significance of magnetic anisotropy in Appalachian sedimentary rocks. In: Steinhart JS, Smith TJ (eds) *The earth beneath the continents*, vol 10. *Geophysical Monographs*, pp 627–648
- Hardebeck JL, Hauksson E (2001) Crustal stress field in southern California and its implications for fault mechanics. *J Geophys Res* 106:21859–21882
- Hirt AM, Lowrie W, Clendenen WS, Kligfield R (1988) The correlation of magnetic anisotropy with strain in the Chelmsford Formation of the Sudbury Basin, Ontario. *Tectonophysics* 145:177–189
- Housen BA, Richter C, van der Pluijm BA (1993) Composite magnetic anisotropy fabrics: experiments, numerical models, and implications for the quantification of rock fabrics. *Tectonophysics* 200:1–12
- Housen BA, Tobin HJ, Labaume P, Leitch EC, Maltman A (1996) ODP leg 156 shipboard science party Strain decoupling across the decollement of the Barbados accretionary prism. *Geology* 24(2):127–130
- Hrouda F (1982) Magnetic anisotropy of rocks and its application in geology and geophysics. *Geophys Surv* 5:37–82

- Hrouda F, Jelinek V, Hruskova L (1990) A package of programs for statistical evaluation of magnetic data using IBM-PC computers. *Eos Trans AGU* 71(43):1289
- Jayangondaperumal R, Thakur VC (2008) Kinematics of coseismic secondary surface fractures on southeastward extension of the rupture zone of Kashmir earthquake. *Tectonophysics* 446:61–76
- Jelinek V (1977) The statistical theory of measuring anisotropy of magnetic susceptibility of rocks and its application. *Brno Geofyzika*
- Jelinek V (1981) Characterization of the magnetic fabrics of rocks. *Tectonophysics* 79:63–67
- Kissel C, Barrier E, Laj C, Lee TO (1986) Magnetic fabric in “undeformed” marine clays from compressional zones. *Tectonics* 5:769–781
- Kligfield R, Owens WH, Lowrie W (1981) Magnetic susceptibility anisotropy, strain and progressive deformation in Permian sediments from the Maritime Alps (France). *Earth Planet Sci Lett* 55:181–189
- Kumar S, Wesnousky SG, Rockwell TK, Briggs RW, Thakur VC, Jayangondaperumal R (2006) Paleoseismic evidence of great surface rupture earthquakes along the Indian Himalaya. *J Geophys Res* 111:B03304. doi:10.1029/2004JB003309
- Lave J, Yule D, Sapkota S, Basant K, Madden C, Attal M, Pandey R (2005) Evidence for a great medieval earthquake (~1100 A.D.) in the central Himalayas, Nepal. *Science* 307:1302–1305
- Lee TQ, Angelier J (2000) Tectonic significance of magnetic susceptibility fabrics in Plio-Quaternary mudstones of southwestern foothills, Taiwan. *Earth Planet Space* 52:527–538
- Lee TQ, Kissel C, Laj, Hornig CS, Lue YT (1990) Magnetic fabric analysis of the Plio Pleistocene sedimentary formations of the coastal range of Taiwan. *Earth Planet Sci Lett* 98:23–32
- Levi S, Nabelek J, Yeats RS (2005) Paleomagnetism-based limits on earthquake magnitudes in northwestern metropolitan Los Angeles, California, USA. *Geology* 33(5):401–404. doi:10.1130/G21190.1
- Levi S, Weinberger R, Alfa T, Eyal Y, Marco S (2006) Earthquake-induced clastic dikes detected by anisotropy of magnetic susceptibility. *Geology* 34(2):69–72. doi:10.1130/G22001.1
- Lüneburg CM, Lampert SA, Lebit HD, Hirt AM, Casey M, Lowrie W (1999) Magnetic anisotropy, rock fabrics and finite strain in deformed sediments of SW Sardinia (Italy). *Tectonophysics* 307:51–74
- Martinez-Diaz JJ (2002) Stress field variation related to fault interaction in a reverse oblique-slip fault: the Alhama de Murcia fault, Betic Cordillera, Spain. *Tectonophysics* 356:291–305
- Nakata T (1972) Geomorphic history and crustal movements of the foothills of the Himalayas, vol 22. *Science Report Tohoku University*, 7th series, pp 39–177
- Nelson KD (1998) The Himalaya and Tibetan Plateau: a perspective from project INDEPTH, paper presented at Geological Society of America, 1998 annual meeting. Geological Society of America, Boulder
- Owens WH (1993) Magnetic fabric studies of samples from Hole 808c, Nankai trough. In: Hill IA, Taira Firth JV (eds) *Proceeding of the ocean drilling program, scientific results, ocean drilling program*, vol 131, pp 301–310
- Parés JM (2004) How deformed are weakly deformed mud rocks? Insights from magnetic anisotropy. In: Martin-Hernandez F, Lüneburg CM, Aubourg C, Jackson M (eds) *Magnetic fabrics: methods and applications*, vol 238. Geological Society, Special Publication, pp 191–203
- Parés JM, van der Pluijm BA (2002) Evaluating magnetic lineations (AMS) in deformed rocks. *Tectonophysics* 350:283–298
- Parés JM, van der Pluijm BA (2003) Magnetic fabrics in low-strain mud rocks: AMS of pencil structures in the Knobs Formation, mud rocks (Valley and Ridge Province, US Appalachians). *J Struct Geol* 25:1349–1358
- Parés JM, van der Pluijm BA, Dinares-Turell J (1999) Evolution of magnetic fabrics during incipient deformation of mudrocks (Pyrenees, northern Spain). *Tectonophysics* 307:1–14
- Philip H, Meghraoui M (1983) Structural analysis and interpretation of the surface deformations of the EL ASNAM earthquake of OCTOBER 10, 1980. *Tectonics* 2(1):17–49
- Rathore JS (1980) The magnetic fabric of some slates from the Borrodale volcanic group in the English Lake District and their correlations with strain. *Tectonophysics* 67:207–220
- Robion P, Grelaud S, Frizon de Lamotte D (2007) Pre-folding magnetic fabrics in fold-and-thrust belts: Why the apparent internal deformation of the sedimentary rocks from the Minervois basin (NE-Pyrenees, France) is so high compared to the Potwar basin (SW-Himalaya, Pakistan)? *Sed Geol* 196:181–200
- Rochette P, Jackson M, Aubourg C (1992) Rock magnetism and the interpretation of the anisotropy of magnetic susceptibility. *Rev Geophys* 30:209–226
- Sagnotti L, Speranza F (1993) Magnetic fabric analysis of the Plio-Pleistocene clayey units of the Sant’ Arcangelo basin, Southern Italy. *Phys Earth Planet Inter* 77:165–176
- Sagnotti L, Faccenna C, Funicello R, Mattei M (1994) Magnetic fabric and structural setting of Plio-Pleistocene clayey units in an extensional regime: the Tyrrhenian margin of central Italy. *J Struct Geol* 16:1243–1257
- Sagnotti L, Speranza F, Winkler A, Mattei M, Funicello R (1998) Magnetic fabric of clay sediments from the external northern Apennines (Italy). *Phys Earth Planet Inter* 105:73–93
- Saint-Bezar B, Hebert RL, Aubourg C, Robion P, Swennen R, Frizon de Lamotte D (2002) Magnetic fabric and petrographic investigation of hematite-bearing sandstone with ramp-related folds: examples from the south Atlas Front (Morocco). *J Struct Geol* 24:1507–1520
- Schwehr K, Tauxe L (2003) Characterization of soft-sediment deformation: detection of cryptoslumps using magnetic methods. *Geology* 31:203–206
- Seeber L, Armbruster J (1981) Great detachment earthquakes along the Himalayan Arc and long-term forecasting, in earthquake prediction. In: Simpson DW, Richards PG (eds) *An international review*. American Geophysical Union, Washington, DC, pp 259–277
- Tarling DH, Hrouda F (1993) *The magnetic anisotropy of rocks*. Chapman and Hall, London
- Valdiya KS (1992) The main boundary thrust zone of the Himalaya, India. *Annal Tect* 6:54–84
- Wesnousky SG, Kumar S, Mohindra R, Thakur VC (1999) Uplift and convergence along the Himalayan Frontal thrust of India. *Tectonics* 18:967–976
- Yeats RS, Hussain A (2006) Surface Features of the Mw 7.6, 8 October 2005 Kashmir earthquake, Northern Himalaya, Pakistan: implications for the Himalayan front. In: *Seismological Society of America annual meeting (SSA)*, San Francisco, CA